Resonance Localized Surface Plasmon Spectroscopy: Sensing Substrate and Inhibitor Binding to Cytochrome P450

Jing Zhao,[†] Aditi Das,[‡] George C. Schatz,*[,†] Stephen G. Sligar,*[,‡] and Richard P. Van Duyne*[,†]

Department of Chemistry, Northwestern University, 2145 Sheridan Road, Evanston, Illinois 60208-3113, and Department of Biochemistry and Chemistry, Beckman Institute for Advanced Science and Technology, University of Illinois Urbana−Champaign, Urbana, Illinois 61801

Received: February 27, 2008; Revised Manuscript Received: June 19, 2008

A sensing method based on resonance localized surface plasmon spectroscopy was developed for low molecular weight substrate and inhibitor molecules binding to heme proteins. Cytochrome P450 proteins have Soret and Q absorption bands in the visible wavelength region. The coupling between the molecular resonance of P450 and the localized surface plasmon resonance (LSPR) of functionalized silver nanoparticles leads to a highly wavelength-dependent LSPR response. Binding of substrate (e.g., camphor) or inhibitor (e.g., imidazole) molecules to a cytochrome P450 causes the absorption band of cytochrome P450 shift to shorter or longer wavelengths, respectively. By monitoring the localized surface plasmon resonance (LSPR) of the nanosensors, the binding of camphor/imidazole to a nanoparticle whose surface is modified with cytochrome P450 protein leads to a wavelength-dependent blue/red shift in the LSPR. The magnitude of the LSPR shift induced by camphor or imidazole is consistent with the Soret band wavelength shift observed in P450 in solution.

Introduction

The interaction between the metal nanoparticles and optical chromophores has been widely used in a variety of applications, such as in molecular plasmonic devices,[1–3] dye sensitized solar cells,[4–6] and biosensing and imaging applications.[7–11] The interaction between chromophore and metal nanoparticles (or thin films) is critical to the understanding of surface-enhanced spectroscopies and improving the performance of chromophore/metal based devices. Recent progress has shown that localized surface plasmon resonance (LSPR) spectroscopy of metallic nanoparticles is a powerful tool to investigate the coupling between the chromophore's molecular resonances and the plasmon resonance modes of the nanoparticles.[3,11–13]

Localized surface plasmon resonance involves the collective oscillation of the conduction electrons in metallic nanostructures excited by electromagnetic radiation.[14–17] The LSPR wavelength of a given nanostructure is extremely sensitive to the local dielectric environment, so a shift in this wavelength upon analyte binding can be used in refractive index sensors.[18–21] Indeed, during the past few years, many LSPR sensors have been developed for chemical/biological targets.[20,22–26] Recently, LSPR sensors have been exploited for analytes with molecular resonances in the visible wavelength region.[11–13]

Based on previous experimental and theoretical studies, strong coupling of molecular chromophore and plasmon resonances is expected when molecules are adsorbed on metal nanostructures.[3,11,13,27,28] When chromophores adsorb on nanoparticles in monolayer concentrations, extinction from plasmon resonance excitation in the nanoparticle greatly exceeds that originating with the chromophore, and the interaction between the chromophore and plasmon is observable through the LSPR wavelength shift. In addition, the LSPR wavelength shift induced by resonant adsorbates is strongly dependent on plasmon wavelength. As a result, the LSPR shift is sensitive to small changes in the resonances of the chromophore that are induced by binding of an additional analyte,[11] by chromophore dimerization,[13] etc. In particular, recent studies demonstrate that LSPR wavelength shifts can be used to detect the spectral changes caused by the electronic structure changes around the heme center in cytochrome P450 proteins due to low molecular weight substrate binding.[11]

Cytochrome P450s are ubiquitous heme iron monooxygenases which activate dioxygen for insertion into an unactivated C−H bond and play important roles in human drug metabolism and hormone biosynthesis.[29] Cytochrome P450s have interesting spectroscopic properties due to the unique molecular structure around the heme active site. The low spin six-coordinate P450 resting state has cysteine thiolate and water as axial ligands. On binding a substrate such as camphor, the water ligand is displaced and the low spin $S = 1/2$ state is converted to a high spin $S = 5/2$ d-electron configuration. On the other hand, the binding of N-donor or O-donor inhibitors, the water ligation is replaced by an N-donor or O-donor atom and the resting ferric P450 remains low spin.[30–33] The ferric iron spin state and the ligation around the iron center in P450 affect its spectroscopic properties.[34,35]

These spectroscopic properties of P450 have been well characterized. The optical spectrum of oxidized CYP101 (a member of the P450 super family isolated from *Psuedomonas putida*) is that of a low-spin ferric hemeprotein with Soret maximum at 417 nm ($\epsilon = 115\,000\ M^{-1}\ cm^{-1}$), β-Q-band at 536 nm ($\epsilon = 10\,600\ M^{-1}\ cm^{-1}$), and a more intense α-Q-band at 569 nm ($\epsilon = 11\,100\ M^{-1}\ cm^{-1}$).[31] Upon addition of substrate, which displaces the coordinated water associated with heme-iron, the spin state of heme-iron changes from low-spin to high spin as monitored by the shift in the Soret band from 417 to 390 nm. There is a decrease in the intensity of the α-Q-band at

* Corresponding authors. George C. Schatz, E-mail: schatz@chem.northwestern.edu. Telephone: (847) 491-5657. Fax: (847) 491-7713; Stephen G. Sligar, E-mail: s-sligar@uiuc.edu. Telephone: (217) 244-7395. Fax: (217) 265-4073; Richard P. Van Duyne, E-mail: vanduyne@northwestern.edu, Telephone: (847) 491-3516. Fax: (847) 491-7713.

[†] Northwestern University.

[‡] University of Illinois Urbana−Champaign.

10.1021/jp801719c CCC: $40.75
Published on Web 07/30/2008

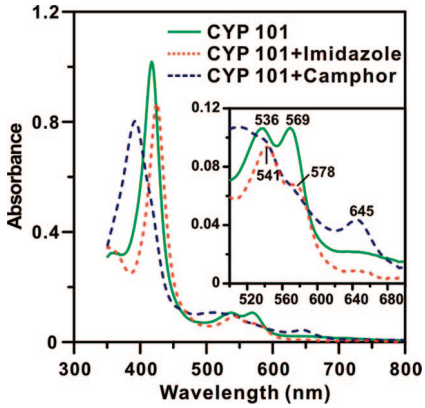

Figure 1. UV−vis absorption spectrum of CYP101 (green solid line), imidazole-bound CYP101 (red dotted line), and camphor-bound CYP101 (blue dashed line). Inset, absorbance of the Q-bands zoomed in the 500∼700 nm wavelength range.

569 nm relative to β-Q-band at 536 nm and the appearance of a charge transfer band at 645 nm. The addition of ligands with nitrogen or oxygen donor atoms causes the Soret band to red shift. In particular, addition of imidazole red-shifts the Soret band to 425 nm because imidazole is a π-donor to ferric porphyrins, donating electrons to the hole in the d_{xz} and d_{yz} orbitals of the iron in the ferric state. The imidazole bound CYP101 has a Soret peak at 425 nm and α-Q-band at 578 nm and β-Q-band at 541 nm.[30,32] The β-Q is more intense than the α-Q-band and therefore the binding of substrate (such as camphor) and inhibitor (such as imidazole) to CYP101 can be spectrally distinguished.[30] The UV−vis absorption spectra of free, camphor-bound and imidazole-bound CYP101are shown in Figure 1.

In this work, we present the development of a LSPR sensor to detect substrate/inhibitor binding to cytochrome P450 and include a detailed study of the coupling between the Soret and Q bands of CYP101 to the LSPR wavelength of Ag nanoparticles and a comparison of the effect of substrate and inhibitor molecule binding to the immobilized CYP101.

Experimental Methods

Materials. Silver shot was purchased from Alfa Aesar (#11357 1−3 mm diameter, Premion, 99.9999%). Tungsten vapor deposition boats were acquired from R.D. Mathis (Long Beach, CA). Polystyrene nanospheres with diameters of 280 ± 4 and 390 ± 19.5 nm were received as a suspension in water (Interfacial Dynamics Corporation, Portland or Duke Scientific, Palo Alto, CA) and were used without further treatment. Fisherbrand no. 2 glass coverslips with 18 mm diameters and the buffer salts ($KH_2PO_4.3H_2O$ and KH_2PO_4) were obtained from Fisher Scientific (Pittsburgh, PA). (1*R*)-Camphor, imidazole, and 11-mercaptoundecanoic acid (11-MUA) were purchased from Sigma-Aldrich and used as received. For all steps of substrate preparation, water purified with cartridges from Millipore (Marlborough, MA) to a resistivity of 18.2 MΩ·cm^{-1} was used. 1-Ethyl-3-[3-dimethylaminopropyl]carbodiimide hydrochloride (EDC) was purchased from Pierce (Rockford, IL).

Protein Expression and Purification. Recombinant wild-type P450cam protein was expressed in *Escherichia coli* and purified as reported[36,37] and stored at −80 °C at ∼100 μM concentration in 50 mM potassium phosphate buffer containing 150 mM potassium chloride salt (pH 7.4), 200 μM camphor, and 20 mM β-mercaptoethanol. Concentrations of CYP101 were determined using extinction coefficients $\epsilon_{391} = 102$ mM^{-1}·cm^{-1} (camphor-bound) or $\epsilon_{417} = 115$ mM^{-1}·cm^{-1} (substrate-free) in aqueous solution. The proteins were made substrate-free by passage through Superdex G-25 column.

Glass Substrate Preparation. Glass substrates were cleaned in piranha solution (1:3 30% H_2O_2/H_2SO_4) for one hour at 80 °C. *(Warning: Piranha reacts violently with organic compounds and should be handled with caution.)* Samples were cooled to room temperature and were then rinsed profusely with deionized (18.2 MΩ·cm) water. Samples were then sonicated in 5:1:1 $H_2O/NH_4OH/30\%$ H_2O_2 and thoroughly rinsed with water. The samples were stored in deionized (18.2 MΩ·cm) water prior to use.

Nanoparticle Preparation. Nanosphere lithography (NSL)[38] was used to create monodisperse, surface-confined Ag nanoparticles. Polystyrene nanospheres (∼2.2 μL) were drop-coated onto the glass substrates and allowed to dry, forming a monolayer in a close-packed hexagonal formation, which served as a deposition mask. The samples were then transferred to the evaporation chamber. The pressure in the vacuum chamber was maintained below 1×10^{-5} Torr during the evaporation and a silver film was evaporated onto the slides. The deposition rate Ag was 1.0 ∼ 1.5 Å/s. A Leybold Inficon XTM/2 quartz crystal microbalance (East Syracuse, NY) was used to measure the thickness of the Ag film deposited over the nanosphere mask, d_m. Following metal deposition, the samples were sonicated for 3−5 min in ethanol to remove the polystyrene nanosphere mask. The perpendicular bisector of the nanoparticles was varied by changing the diameter of the nanospheres used. The height of the nanoparticles was varied by depositing varying amounts of Ag onto the sample. These two parameters were varied to alter the LSPR peak position throughout the visible region of the spectrum as previously described.[38]

Nanoparticle Solvent Annealing and Functional Immobilization. For each experiment, the sample was stabilized and functionalized in a home-built flow cell. Immediately following nanospheres removal, the samples were placed in 1 mM of 11-MUA ethanol solution for 24∼48 h. This time was determined to produce the repeatable and approximately full monolayer coverage of 11-MUA. After incubation, the nanoparticle samples were rinsed thoroughly with neat ethanol and dried by flowing N_2 gas through the sample cell. Samples were then activated using 10 mM EDC and then they were incubated in 8 μM CYP101 for 1 h. After incubation, the nanoparticle samples were rinsed with deionized (18.2 MΩ·cm) water and dried by flowing N_2 gas through the sample cell. Finally, the samples were incubated in 200 μM camphor buffer solution or 1 mM imidazole buffer solution for 30 min. After incubation, the nanoparticle samples were rinsed with deionized (18.2 MΩ·cm) water and dried by flowing N_2 gas through the sample cell.

Ultraviolet−Visible Spectroscopy. Macroscale UV−vis extinction measurements were collected using an Ocean Optics (Dunedin, FL) SD2000 fiber optically coupled spectrometer with a CCD detector and a Cary 300 Bio UV−vis spectrophotometer. All spectra in this study are macroscopic measurements performed in standard transmission geometry with unpolarized light. The extinction spectra of the same sample acquired from the two spectrometers were calibrated.

Results and Discussion

Coupling between P450 Resonances and LSPR. The CYP101 UV−vis spectrum is shown in Figure 1. The substrate free CYP101 has a Soret band at 417 nm with extinction coefficient $\epsilon = 115$ mM^{-1} cm^{-1}, a less intense α-Q-band at

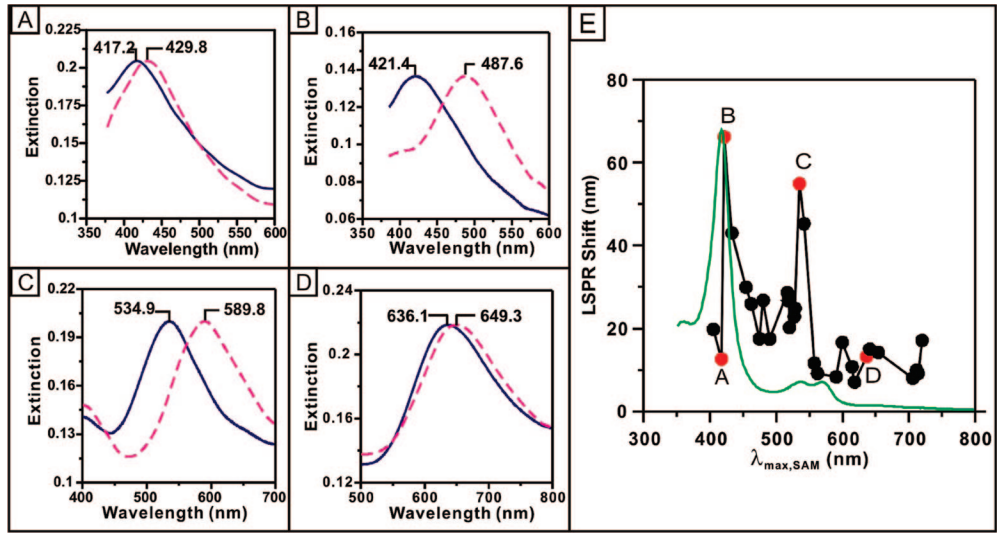

Figure 2. Influence of CYP101 on the LSPR shift of 11-MUA SAM functionalized Ag nanoparticles and representative LSPR spectra. (A−D) LSPR spectra of Ag nanoparticles (associated with points A−D in panel E) before (blue line) and after CYP101 binding (pink dotted line). Labeled are the LSPR peak positions of the spectra. (E) Wavelength-dependent LSPR shift induced by CYP101 vs the LSPR wavelength of 11-MUA SAM functionalized Ag nanoparticles. Solid black line with filled dots is a plot of the LSPR shift (nm) vs LSPR position of 11-MUA Ag nanoparticles. The green solid line is the absorption spectrum of the CYP101 (arbitrary scaling).

569 nm with $\epsilon = 11.1$ mM^{-1} cm^{-1} and β-Q-band at 536 nm with $\epsilon = 10.6$ mM^{-1} cm^{-1}. To study the coupling of P450 resonances with plasmon resonance of the nanoparticles, nanoparticles with LSPR through 400∼700 nm were fabricated by nanosphere lithography (NSL) by varying the nanosphere diameter and deposited metal thickness.[20,22,39,40] The nanoparticles were then functionalized with a self-assembled monolayer (SAM) of 11-mercaptoundecanoic acid (11-MUA). With the aid of 1-ethyl-3-[3-dimethy-aminopropyl] carbodiimide hydrochloride, the amine functional groups on the surface exposed arginine/lysine residues in cytochrome P450cam were covalently bound to the carboxyl terminated groups on 11-MUA.[20] The LSPR of the samples during each experimental step was monitored using UV−vis extinction spectroscopy in a N_2 environment.

Figure 2A−D shows the representative spectra of MUA-functionalized nanoparticles and after CYP101 adsorption. Adsorption of CYP101 causes a red-shift in the LSPR of the nanoparticles. Previous work has demonstrated that the LSPR response of nanoparticles to resonant adsorbates is wavelength-dependent.[11−13] Hence, a series of nanoparticles with different LSPR were fabricated with NSL, and their response to binding CYP101 was explored. The LSPR shift induced by CYP101 versus LSPR of MUA-functionalized nanoparticles ($\lambda_{max,SAM}$) is plotted in Figure 2E. When $\lambda_{max,SAM}$ is displaced from the heme CYP101 resonance wavelengths (>590 nm), an average LSPR shift of ∼11 nm is observed when CYP101 binds to the nanoparticles. When $\lambda_{max,SAM}$ overlaps with the Soret band of CYP101 at 417 nm, a small LSPR shift of 12.6 nm was observed (spectra shown in Figure 2A), which is consistent with the previous studies.[11−13] When $\lambda_{max,SAM}$ is slightly to the red of the Soret band, an amplified LSPR shift as large as 66 nm was obtained (spectra shown in Figure 2B). The LSPR shift is amplified by 6 times compared to the average LSPR shift at off resonance wavelength. When $\lambda_{max,SAM}$ is shifted to the red of the Soret band, the LSPR shift gradually decreases to ∼20 nm.

An interesting phenomenon was observed that when $\lambda_{max,SAM}$ is close to the β-Q-band of CYP101, the LSPR shift increases dramatically to 55 nm (spectra shown in Figure 2C). This behavior indicates that there is strong coupling between the β-Q-band and LSPR excitation. Note that although the absorption coefficient of the β-Q-band is 10 times smaller than that of the Soret band, the magnitude of the shift from the coupling between the β-Q-band and LSPR is comparable to the shift induced by Soret band coupling. This is partly due to the wavelength dependence of the LSPR field enhancement, which, even for nonresonant adsorbates, leads to a linear increase in wavelength shift with plasmon resonance wavelength. For example, when a monolayer of benzenethiol molecules adsorb on Ag nanoparticles with different plasmon resonance wavelength, it leads to a ∼35 nm shift when the nanoparticles' LSPR is at 475 nm and a ∼50 nm LSPR shift at 725 nm.[13] However, when $\lambda_{max,SAM}$ is further red-shifted to the α-Q-band of CYP101, the LSPR shift is ∼ 10 nm, close to the average LSPR shift at off-resonance wavelengths. This behavior suggests that the α-Q-band is weaker relative to β-Q when CYP101 is adsorbed on the surface than in solution. The ratio of α-Q/β-Q intensities is known to vary from one protein to another due to strong sensitivity of this ratio (which is determined by vibronic interactions) to small variations in the heme group excited-state properties.[41,42]

P450 LSPR Sensor Response to Low Molecular Weight Substrate and Inhibitor. The cytochrome P450 CYP3 enzyme family plays a central role in drug metabolism. In particular, CYP3A4 is responsible for the metabolism of more than 50% of currently marketed drugs and is considered the central focus of clinically manifested drug-drug interactions.[43] The binding of inhibitory drugs such as the antifungal drugs fluconazole, itraconazole, micafungin, miconazole, and voriconazole to cytochrome P450s in humans can dramatically modulate the activity of other therapeutics. The development of an ultrasensitive, label free detection method such as LSPR for detection of binding of the drug molecules to cytochrome P450s could have a significant impact on drug discovery research.[29,44]

Previous studies have shown that LSPR is sensitive to the electronic structure change in the adsorbed species.[11,13] When different drug molecules interact with P450 proteins, they induce a change in the absorption spectrum of P450. The wavelength of the Soret and Q bands of cytochrome P450s are determined

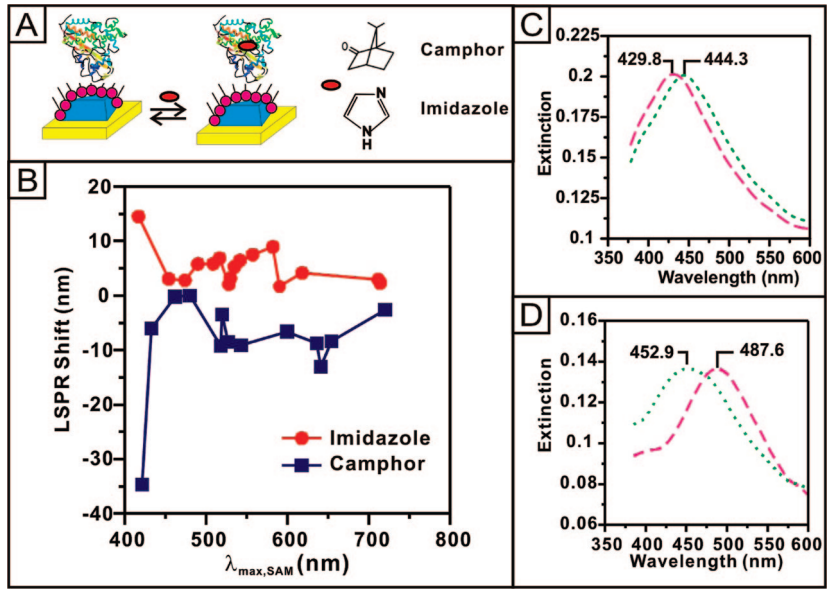

Figure 3. (A) Schematic illustration of small molecule binding to CYP101 receptors on 11-MUA functionalized Ag nanoparticles. Inset shows the molecular structure of camphor and imidazole. (B) The wavelength-dependent LSPR shift induced by imidazole (red line with red dots) and camphor (blue line with squares). (C) Representative LSPR spectra of nanoparticles with CYP101 before (a, pink dashed line) and after (b, green dotted line) camphor binding. (D) Representative LSPR spectra of nanoparticles with CYP101 before (pink dashed line) and after (green dotted line) imidazole binding.

by the ligand coordination of heme-iron. Figure 1 shows the UV−vis spectra of substrate-free CYP101 (green solid line), camphor-bound CYP101 (blue dashed line) and imidazole-bound CYP101 (red dotted line). From Figure 1, when the substrate molecule camphor binds to CYP101, it replaces the coordinated water and shifts the spin state of heme-iron to high spin. This binding induces the Soret band to shift from 417 to 391 nm. When an inhibitor molecule with N-donor atoms such as imidazole (MW = 64.08 g/mol), binds to CYP101, there is electron donation from imidazole to heme-iron which induces a red shift in the Soret band from 417 to 425 nm.[30,32,34,35,45] The LSPR wavelength is extremely sensitive to the electronic resonances of the adsorbates; therefore, one should be able to detect the above binding events by fabrication of LSPR sensors at appropriate wavelengths.

The LSPR sensing scheme is illustrated in Figure 3A. After P450 is immobilized on the nanoparticle surface, camphor/imidazole is further exposed to the protein. Figure 3C-D shows the spectra before and after camphor or imidazole binds to CYP101, respectively. When camphor binds to CYP101, it induces a blue shift in the LSPR; while when imidazole binds to CYP101, it induces a red shift in the LSPR. The blue/red LSPR shift response is consistent with the blue/red electronic resonance shifts induced by the binding of camphor/imidazole.

Since the LSPR response to resonant analyte is wavelength-dependent, samples with different LSPR wavelengths were tested. The LSPR response of the CYP101 receptor to camphor (blue squares) and imidazole (red dots) versus $\lambda_{max,SAM}$ is summarized in Figure 3B. At wavelengths away from the Soret band resonance ($\lambda_{max,SAM} > 460$ nm), camphor induces an average blue shift of ~6 nm. However when $\lambda_{max,SAM}$ is slightly red of the P450 resonance, a blue shift as large as 34 nm (a factor of 5 amplification over the nonresonant result) is observed. As for imidazole, away from the Soret band resonance ($\lambda_{max,SAM} > 460$ nm), an average red shift of 4.7 nm is induced. However when $\lambda_{max,SAM}$ is close to the P450 optical resonance, a 3× amplified LSPR shift of 14.5 nm is observed. Note that no significant shift on binding camphor or imidazole is observed at the Q-band wavelengths. This is consistent with the small wavelength changes seen in Figure 1 for the Q-bands associated with camphor or imidazole binding.

The amplitude of the LSPR shift amplification is larger for camphor binding (5×) than for imidazole binding (3×). This can be described by analyzing the coupling of molecular resonances with LSPR. When camphor binds to CYP101, the Soret band is blue-shifted by 27 nm (from 417 to 390 nm). Nanoparticles with LSPR wavelengths slightly red of the CYP101 resonance are strongly coupled to the Soret band of substrate free CYP101 where a large LSPR shift is expected upon protein binding to the nanoparticle. However, the same nanoparticles (with the absorption slightly red of the CYP101 417 nm resonance) do not couple strongly to camphor-bound CYP101 resonance at 390 nm where a relatively small LSPR shift is expected on binding camphor bound protein to the nanoparticle. Therefore, the net LSPR shift induced by camphor-bound CYP101 is much smaller than the LSPR shift caused by camphor-free CYP101. Thus, a large blue shift in the LSPR is observed at the CYP101 resonance wavelength when camphor binds to CYP101.

When imidazole binds to CYP101 there is an 8 nm red shift (from 417 to 425 nm) in its Soret band. The magnitude of the shift is much smaller than that observed when camphor binds, which means the electronic resonances of CYP101 and imidazole-bound CYP101 are closer. When nanoparticles couple strongly to imidazole-bound P450, they also couple strongly to free CYP101. Therefore, the difference between the LSPR shift induced by imidazole-bound CYP101 and free CYP101 is relatively small and only a relatively small red-shift is observed for imidazole binding.

Previous studies have shown that the LSPR shift induced by a resonant adsorbate is proportional to the real part of the refractive index of the adsorbate. Further, this refractive index can be estimated using a Kramers−Kronig transformation procedure that is applied to the solution absorption spectrum.[12,13] The LSPR shift predicted from this approach agrees qualitatively with the experimental data from several resonant analytes.[12,13] More quantitative analysis based on electrodynamics calculations can also be implemented, however there is always uncertainty

in determining the resonant adsorbate index, so the more qualitative methods should be adequate for understanding the connection of solution spectra to plasmon wavelength shifts. Here, we apply this approach to study the LSPR shift induced by camphor and imidazole binding to CYP101. A detailed description of the method can be found in the Supporting Information and previous publications.[12,13,25] Figure S1-A in the Supporting Information shows the calculated change in the real part of the refractive index (Δn) of free and camphor/imidazole bound CYP101 relative to the their refractive index at nonresonant wavelengths. Δn was obtained from Kramers−Kronig transformation using the absorption spectra in solution. The LSPR shift induced by camphor/imidazole binding to CYP101 was then calculated using eq 1 in the Supporting Information and plotted in Figure S1-B. From the plot, the predicted LSPR shift induced by camphor is negative corresponding to a blue shift while that by imidazole in positive, corresponding to a red shift. Furthermore, the calculated LSPR shift is wavelength-dependent. The prediction agrees qualitatively with the experimental results shown in Figure 3B, confirming that the LSPR shift induced by small molecule binding to the protein is correlated to the change in the solution absorption spectra.

Conclusion

The shifts in localized surface plasmon resonance wavelengths due to substrate binding have been demonstrated as a platform for signal transduction and the detection of low molecular weight molecule binding to cytochrome P450 proteins. The substrate free CYP101 shows an amplified LSPR shift from coupling of the Soret and Q bands of P450 with the LSPR. Amplified spectral response to substrate/inhibitor binding is achieved when the LSPR of the silver nanosensor is optimized to be close to the Soret band of the protein. The different binding mechanisms of substrate/inhibitor result in different spectral shifts, with camphor shifting blue and imidazole shifting red. The shift direction and magnitude is consistent with P450 spectral shift direction and magnitude.

This study demonstrates the significant sensitivity of LSPR wavelengths to the interaction of small molecule substrates that bind to proteins adsorbed on the surface of silver nanoparticles. The extreme sensitivity of LSPR wavelength to adsorbate electronic transitions makes it possible to use this technique to detect low molecular weight adsorbates in relatively low coverage. Application of this finding to the screening for inhibitors of human cytochrome P450s is under investigation based on these results. This discovery will provide guidance to the design of plasmonic switches that can be turned on/off by small molecule binding events.

Acknowledgment. The authors gratefully acknowledge support from the National Science Foundation (EEC-0647560, CHE-0414554, DMR-0520513, and BES-0507036), the DTRA JSTO Program (FA9550-06-1-0558), AFOSR/DARPA Project BAA07-61 (FA9550-08-1-0221), and the National Cancer Institute (1 U54 CA119341-01). Any opinions, findings, and conclusions or recommendations expressed in this material are those of the authors and do not necessary reflect those of the National Science Foundation.

Supporting Information Available: Detailed description of Kramers−Kronig transformation and the relationship between LSPR shift and refractive index. This material is available free of charge via the Internet at http://pubs.acs.org.

References and Notes

(1) Becke, A. D. *Phys Rev A* **1988**, *38*, 3098.
(2) Leroux, Y. R.; Lacroix, J. C.; Chane-Ching, K. I.; Fave, C.; Felidj, N.; Levi, G.; Aubard, J.; Krenn, J. R.; Hohenau, A. *J. Am. Chem. Soc.* **2005**, *127*, 16022.
(3) Wurtz, G. A.; Evans, P. R.; Hendren, W.; Atkinson, R.; Dickson, W.; Pollard, R. J.; Zayats, A. V.; Harrison, W.; Bower, C. *Nano Lett.* **2007**, *7*, 1297.
(4) Gratzel, M. *Nature* **2001**, *414*, 338.
(5) Gratzel, M. *MRS Bull.* **2005**, *30*, 23.
(6) Martinson, A. B. F.; McGarrah, J. E.; Parpia, M. O. K.; Hupp, J. T. *Phys. Chem. Chem. Phys.* **2006**, *8*, 4655.
(7) Lee, H. J.; Nedelkov, D.; Corn, R. M. *Anal. Chem.* **2006**, *78*, 6504.
(8) Lin, H. Y.; Chen, C. T.; Chen, Y. C. *Anal. Chem.* **2006**, *78*, 6873.
(9) Fujii, E.; Koike, T.; Nakamura, K.; Sasaki, S.; Kurihara, K.; Citterio, D.; Iwasaki, Y.; Niwa, O.; Suzuki, K. *Anal. Chem.* **2002**, *74*, 6106.
(10) Kurihara, K.; Nakamura, K.; Hirayama, E.; Suzuki, K. *Anal. Chem.* **2002**, *74*, 6323.
(11) Zhao, J.; Das, A.; Zhang, X.; Schatz, G. C.; Sligar, S. G.; Van Duyne, R. P. *J. Am. Chem. Soc.* **2006**, *128*, 11004.
(12) Haes, A. J.; Zou, S.; Zhao, J.; Schatz, G. C.; Van Duyne, R. P. *J. Am. Chem. Soc.* **2006**, *128*, 10905.
(13) Zhao, J.; Jensen, L.; Sung, J. H.; Zou, S. L.; Schatz, G. C.; Van Duyne, R. P. *J. Am. Chem. Soc.* **2007**, *129*, 7647.
(14) Kreibig, U.; Gartz, M.; Hilger, A.; Hovel, H. Optical investigations of surfaces and interfaces of metal clusters. In *Advances in Metal and Semiconductor Clusters*; Duncan, M. A., Ed.; JAI Press Inc.: Stamford, CT, 1998; Vol. 4, pp 345−393.
(15) Kreibig, U.; Vollmer, M., *Cluster Materials*; Springer-Verlag: Heidelberg, Germany, 1995; Vol. 25, p 532.
(16) Schatz, G. C.; Van Duyne, R. P. Electromagnetic Mechanism of Surface-Enhanced Spectroscopy. In *Handbook of Vibrational Spectroscopy*; Chalmers, J. M., Griffiths, P. R., Eds.; Wiley: New York, 2002; Vol. 1, pp 759−774.
(17) Willets, K. A.; Van Duyne, R. P. *Annu. Rev. Phys. Chem.* **2007**, *58*, 267.
(18) Jensen, T. R.; Schatz, G. C.; Van Duyne, R. P. *J. Phys. Chem. B* **1999**, *103*, 2394.
(19) Kreibig, U.; Gartz, M.; Hilger, A. *Ber. Bunsen-Ges.* **1997**, *101*, 1593.
(20) Haes, A. J.; Van Duyne, R. P. *J. Am. Chem. Soc.* **2002**, *124*, 10596.
(21) Zhao, J.; Zhang, X. Y.; Yonzon, C. R.; Haes, A. J.; Van Duyne, R. P. *Nanomedicine* **2006**, *1*, 219.
(22) Haes, A. J.; Chang, L.; Klein, W. L.; Van Duyne, R. P. *J. Am. Chem. Soc.* **2005**, *127*, 2264.
(23) McFarland, A. D.; Van Duyne, R. P. *Nano Lett.* **2003**, *3*, 1057.
(24) Qi, Z. M.; Honma, I.; Zhou, H. S. *Opt. Lett.* **2006**, *31*, 1854.
(25) Riboh, J. C.; Haes, A. J.; McFarland, A. D.; Yonzon, C. R.; Van Duyne, R. P. *J. Phys. Chem. B* **2003**, *107*, 1772.
(26) Yonzon, C. R.; Jeoungf, E.; Zou, S. L.; Schatz, G. C.; Mrksich, M.; Van Duyne, R. P. *J. Am. Chem. Soc.* **2004**, *126*, 12669.
(27) Ambjornsson, T.; Mukhopadhyay, G.; Apell, S. P.; Kall, M. *Phys. Rev. B* **2006**, *73*, 085421.
(28) Wiederrecht, G. P.; Wurtz, G. A.; Hranisavljevic, J. *Nano Lett.* **2004**, *4*, 2121.
(29) *Cytochrome P450: Structure, Function, and Mechanism*, 3rd ed.; Kluwer Academic/Plenum: New York, 2005; pp 247−322.
(30) Dawson, J. H.; Andersson, L. A.; Sono, M. *J. Biol. Chem.* **1982**, *257*, 3606.
(31) Denisov, I. G.; Makris, T. M.; Sligar, S. G.; Schlichting, I. *Chem. Rev.* **2005**, *105*, 2253.
(32) Sligar, S. G. *Biochemistry* **1976**, *15*, 5399.
(33) Das, A.; Grinkova, Y. V.; Sligar, S. G. *J. Am. Chem. Soc.* **2007**, *129*, 13778.
(34) Loew, G. H.; Harris, D. L. *Chem. Rev.* **2000**, *100*, 407.
(35) Harris, D.; Loew, G. *J. Am. Chem. Soc.* **1993**, *115*, 5799.
(36) Gunsalus, I. C.; Wagner, G. C. *Methods Enzymol.* **1978**, *52*, 166.
(37) Makris, T. M.; von Koenig, K.; Schlichting, I.; Sligar, S. G. *Biochemistry* **2007**, *46*, 14129.
(38) Haynes, C. L.; Van Duyne, R. P. *J. Phys. Chem. B* **2001**, *105*, 5599.
(39) Malinsky, M. D.; Kelly, K. L.; Schatz, G. C.; Van Duyne, R. P. *J. Am. Chem. Soc.* **2001**, 123.
(40) Riboh, J. C.; Haes, A. J.; McFarland, A. D.; Yonzon, C. R.; Van Duyne, R. P. *J. Phys. Chem. B* **2003**, 107.
(41) Eaton, W. A.; Hochstrasser, R. M. *J. Chem. Phys.* **1968**, *49*, 985.
(42) Eaton, W. A.; Hofrichter, J. *Methods Enzymol.* **1981**, *76*, 175.
(43) Guengerich, F. P. *Annu. Rev. Pharmacol. Toxicol.* **1999**, *39*, 1.
(44) Zlokarnik, G.; Grootenhuis, P. D. J.; Watson, J. B. *Drug Discovery Today* **2005**, *10*, 1443.
(45) Hanson, L. K.; Eaton, W. A.; Sligar, S. G.; Gunsalus, I. C.; Gouterman, M.; Connell, C. R. *J. Am. Chem. Soc.* **1976**, *98*, 2672.

JP801719C